Analysis of Space Charge and Dead Zone Effects in the $\mathcal{TWIST}$ Spectrometer

by

Brynle Barrett

A THESIS SUBMITTED IN PARTIAL FULFILMENT OF
THE REQUIREMENTS FOR THE DEGREE OF

BACHELOR OF SCIENCE

in

Physics

(Department of Physics and Astronomy, Dr. A.J. Sarty supervising faculty)

.....

.....

.....

.....

.....

SAINT MARY'S UNIVERSITY

April 1, 2005

Abstract

Analysis of Space Charge and Dead Zone effects in the $\mathcal{TWIST}$ Spectrometer, by *Brynle Barrett*, submitted on April 1, 2005:

Multi-wire chamber ionization detectors experience effects from space charges due to high energy loss of the radiative particles that penetrate them. One of these effects is that due to the dead zone—the region near a primary ionization path that becomes non-responsive to a subsequent particle traversal. This thesis reports a thorough study of the dead zone produced by μ^+ in the proportional counters closest to the target stop in the $\mathcal{TWIST}$ spectrometer (PC5 and PC6), with emphasis placed on the method of analysis and the use of raw data to measure dead zone effects.

Two parameters that describe the properties of a dead zone are the dead length, L_{dead}, which is the average length along a wire in the proportional counter that becomes unresponsive, and the healing time, τ_h, which is the average time it takes for a dead zone to become responsive again. The dead lengths and healing times for the dead zones in PC5 and PC6 were computed from raw data and are listed in Table 1. Brief descriptions are also given of the $\mathcal{TWIST}$ experiment and the physics of dead zones.

	L_{dead} (cm)	τ_h (ns)
PC5	0.2520 ± 0.0101	1799 ± 70
PC6	0.4297 ± 0.0039	2521 ± 31

Table 1: Final Results for L_{dead} and τ_h of dead zones in PC5 and PC6

Contents

List of Figures

List of Tables

Chapter 1

A Brief Introduction to TRIUMF and $\mathcal{TWIST}$

The work reported in this thesis represents research performed over the summer of 2004 at the TRIUMF laboratory in Vancouver, BC. The primary focus is on a particular type of response observed in proportional counter detectors used in a spectrometer for the $\mathcal{TWIST}$ experiment.

This chapter provides background information to give appropriate context for this research project. The first section overviews the TRIUMF laboratory and the basics of the $\mathcal{TWIST}$ experiment. A detailed description of the mechanism of particle detection in wire chambers is then given, since this is a prerequisite for understanding the effect of space charges in wire chambers. Finally, the goal of this research is defined, followed by a short description of the requirements for completing the work.

1.1 An Overview of the TRIUMF Facility

TRIUMF (**TRI** **U**niversity **M**eson **F**acility) is Canada's premier scientific research facility. It is an international scientific institution which helps serve the needs of many scientists across Canada. Originally supported by three joint member universities, there are now a total of six joint members and seven associate members (including Saint Mary's University) as listed in Table 1.1. [11]

TRIUMF is financially supported by the NRC (**N**ational **R**esearch **C**ouncil) via a five-year renewable allowance provided by the federal government. The current funding cycle covers the 2000-2005 period, and work is underway to develop a new scientific plan for the upcoming funding cycle of 2005-2010.

Joint Venture Members	Associate Members
The University of Alberta	The University of Guelph
The University of British Columbia	The University of Manitoba
Carleton University	McMaster University
Simon Fraser University	L'Université de Montréal
The University of Toronto	Queen's University
The University of Victoria	The University of Regina
	Saint Mary's University

Table 1.1: University Members of TRIUMF

TRIUMF uses a type of particle accelerator called a "cyclotron" which exploits the properties of charged particles moving in electric and magnetic fields to accelerate them in a spiral pattern until they reach sufficiently high energy. The cyclotron at TRIUMF is the largest and most complex cyclotron in the world [10]. It accelerates protons to speeds up to three quarters the speed of light, corresponding to kinetic energies of about 480 MeV. It is also the largest cyclotron that can *ever* be built using ferromagnetic material as the source of magnetism (due to the constraints in size and shape of cyclotrons built with these materials).

The accelerated protons are directed out of the cyclotron where they bombard "targets" of different materials. At such high energies and speeds, the protons hitting the targets cause nuclei to break up into protons and neutrons, with other kinds of charged particles called "pions" and "muons" also being emitted. These secondary charged particles can then be accelerated and used to bombard targets and initiate nuclear reactions, similar to the primary proton reactions.

TRIUMF undertakes a wide variety of materials studies. It is one of the largest producers of rare isotopes, specifically short-lived isotopes of intermediate mass. These are of particular interest to astrophysicists because they are a means of studying the interactions that take place between heavy nuclei in stars and supernovae. Over the past ten years a facility has been built at TRIUMF that creates and isolates these nuclei. It is called the ISAC (**I**sotope **S**eperator and **AC**celeration) facility.

Aside from nuclear physics experiments, TRIUMF also has a center for the practical applications of its research. It is the only center in Canada that uses proton therapy to treat eye cancers. TRIUMF researchers have built a PET (**P**ositron **E**mission **T**omograph) scanner that specializes in brain scans. It is one of three operating in Canada, and is used at the UBC hospital on campus.

With its ability to create radioactive isotopes, TRIUMF develops new radiopharmaceuticals for use in hospitals around the world. TRIUMF researchers have pioneered the packaging and transportation of these goods on an international level.

1.2 The $\mathcal{TWIST}$ Experiment

A variety of experiments are currently underway at TRIUMF, one of which is named $\mathcal{TWIST}$: the **T**RIUMF **W**eak **I**nteraction **S**ymmetry **T**est. [1] As implied by its title, $\mathcal{TWIST}$ is designed to test a fundamental symmetry of nature. In subatomic physics, a symmetry is a property held by particles such that, when observed from a different point of view (through a mirror, for example), there exists a similarity. These symmetries predict the way particles interact with each other, and often have a hidden meaning for understanding the instrinsic properties of particles.

$\mathcal{TWIST}$ is designed to accurately measure the distributions in angle and energy of positrons emitted from decaying muons. The decay of a muon is an example of the "weak interaction", one of the fundamental forces of nature. Similar to the electromagnetic interaction, it can be calculated very precisely, requiring only a small number of measured input parameters. Unlike beta decay, the muon does not involve any strongly interacting particles when it undergoes decay, so it is free of any complications added by the strong interaction (which is a much less precisely understood force of nature that governs the interaction, for example, between protons and

[1] TRIUMF has an experiment referencing system like most other scientific institutions. $\mathcal{TWIST}$s reference number is E614.

neutrons).

A very general space-time symmetry is predicted for the weakly interacting muon decay, and it predicts a specific distribution in angle and energy for the decay positrons. Here the angle of the positron is measured with respect to the muon spin direction. But to date, only a subset of the symmetries provided by the general case have actually been observed. This limitation is considered to be evidence of an even more restrictive and specific underlying symmetry, but what this symmetry is, and why it is so restrictive, is unknown.

Today physicists use the "Standard Model" to predict such observations related to the interaction and/or decay of subatomic particles, but it is considered to be only an approximation to a more complete and correct theory that has yet to be constructed. To help narrow down the options of the correct theory, physicists look for test cases in which the Standard Model might fail. TWIST is one of these tests; it looks for symmetry properties of the weak interaction that are not contained in the Standard Model. As alluded to above, this can be done by accurately measuring the distribution in angle and energy of positrons resulting from muon decay, and using this data to precisely calculate certain parameters describing the distributions. The specific descriptive parameters in this case are called the "Michel Parameters". Precise determination of their values from TWIST data may reveal deviations from the theoretical values predicted by the Standard Model, thus revealing new physics.

1.3 The TWIST Spectrometer

The TWIST spectrometer consists of a superconducting solenoid magnet, which produces a uniform 2T magnetic field [2]. TRIUMFs M13 beamline is comprised of positive muons that are electromagnetically separated from a pion decay, which comes from bombarding a target with protons from the cyclotron. The M13 beamline is

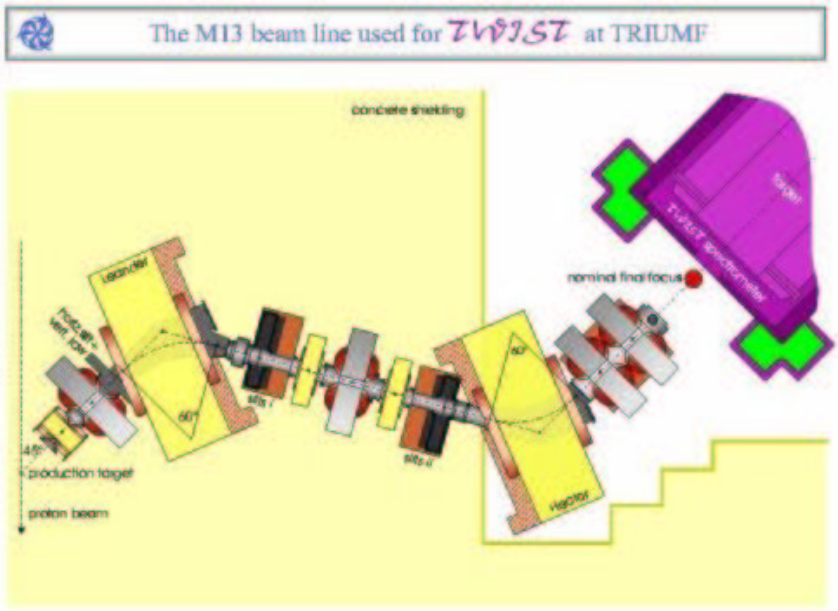

Figure 1.1: Electromagnetic seperation of muons in TRIUMFs M13 beamline
Courtesy of TRIUMF

shown in Figure 1.1. Since the μ^+ come from previous pion decays, they are obtained in a polarized state. The muons are then accelerated towards the center of the solenoid and fired along a direction defined to be the positive z-direction.

The M13 beamline is the source of muons needed for the experiment, the goal of which is to measure the four Michel parameters (ρ, η, δ, and ξ) discussed above that are related to the properties of the fundamental weak interaction responsible for positive muon decay. By finding the four Michel parameters to a greater precision than ever before measured, TWIST will be able to observe any deviations in reality from the Standard Model. However, the challenge faced by such precision tests of an already very successful model is to take all possible steps to avoid having the resulting comparison be limited by systematic uncertainties. The purpose of this study is therefore aimed at finding the systematic uncertainty created in the measurement of the Michel parameters due to dead zones in the TWIST spectrometer.

The spectrometer is designed such that incident muons travel through the up-

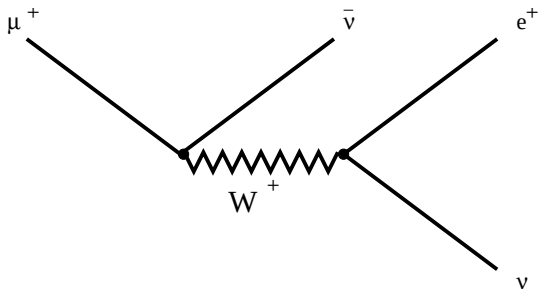

Figure 1.2: Feynman Diagram for positive muon decay: $\mu^+ \rightarrow e^+ + \bar{\nu}_\mu + \nu_e$

stream half of the spectrometer and then decay in a target (located at a position defined as $z = 0$ cm). A muon decays into a positron, an electron neutrino and a muon anti-neutrino, as illustrated in Figure 1.2. Once emitted, the positron creates tracks in either the upstream or downstream wire chambers.

As shown in Figures 1.3 and 1.6, inside the solenoid are 56 planes of wire chambers (labeled in the figures as either "PC" or "DC"), each oriented in a particular direction in order to measure the positions of muon and positron tracks. There are two types of wire chambers in the spectrometer: Proportional Counters (PCs) and Drift Chambers (DCs). They each serve a specific, and different, purpose.

The DCs are placed near the center of the upstream and downstream chambers. They contain a *slow* gas (i.e. the electrons produced in the gas when muons or positrons pass through take a relatively long time to drift to the anode wire). This makes the width of the output electrical pulses (induced in the chamber by these created electron-ion pairs) much longer than the pulses induced in the PCs. Thus, the DCs give a more precise measurement of the ion's drift time. These drift time measurements give a precise calculation of the positions at which the events occurred (i.e. the position in the chamber where a muon or positron traversed). The improved positions are then used for the least squares fitting of the positron tracks in both the upstream and downstream chambers; the positrons follow a helical trajectory due to the solenoidal magnetic field they experience.

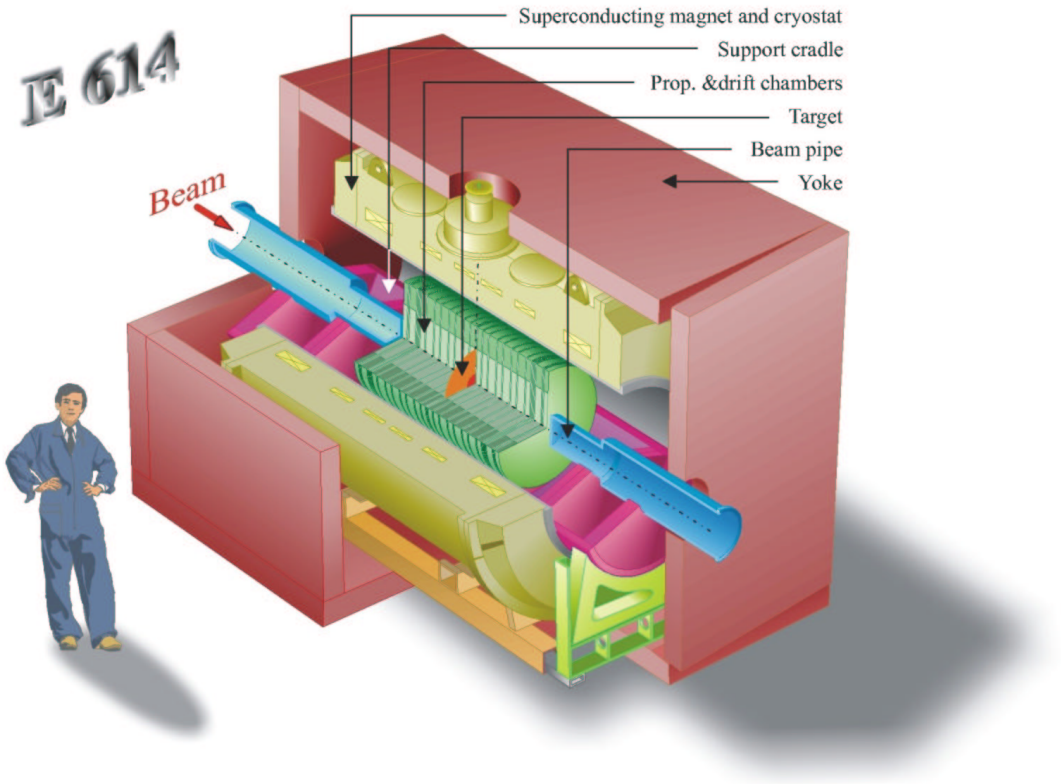

Figure 1.3: TWIST Spectrometer
Courtesy of TRIUMF and TWIST

In order to discuss the dynamics of particles inside the TWIST spectrometer, a discussion of the unique coordinate system used by the experiment is needed. As illustrated in Figure 1.4, a typical multi-wire chamber inside the TWIST spectrometer is rotated by a multiple of $\pi/2$, in this case the rotation angle is 45°. Due to this rotation, a standard cartesian (u, v) coordinate system rotated by 45° relative to the horizontal x-axis is used as the basis for describing particle dynamics. [2]

Figure 1.4 also shows how the wires are divided into different "cells" inside each plane. Although there is no physical boundary dividing one cell from the next, the electric field induced by the charged cathode planes has the effect of isolating charged

[2]The wire chambers are rotated relative to horizontal in this way in order to reduce the sagging of the wires due to gravity.

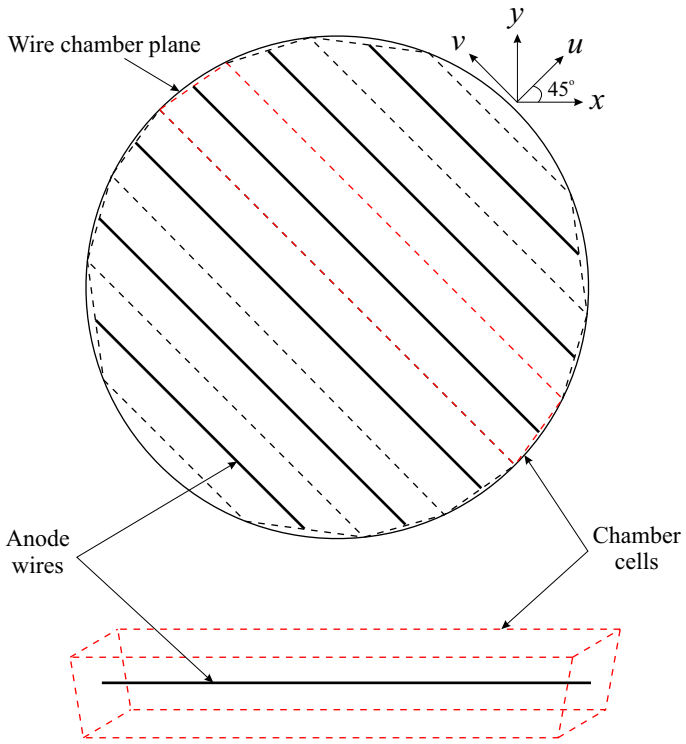

Figure 1.4: Illustration of a wire chamber U-plane and its orientation which determines the coordinate system used by TWIST

particles to a region around particular wire, as shown in Figure 1.5. Since each region is of similar size and shape, they can be treated as single "cells". The entire volume of each plane is filled with a pressurized gas from which the ions are produced.

The plane shown in this figure is called a "U-plane" because the wires run in the v-direction and measure ionization in the u-direction. The real wire chamber planes have a much higher density of wires per plane than shown in Figure 1.4, this will be discussed in Chapter 2.

Recall that, in a uniform magnetic field along the z-axis, the equation of motion of a charged particle is a helix, and the most general form is given by equations (1.1)

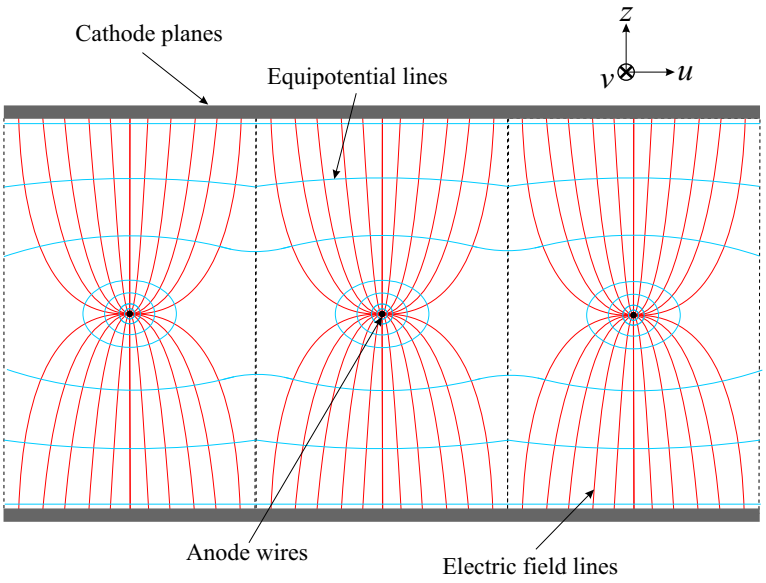

Figure 1.5: Illustration of the $\vec{E}$-field geometry produced by planar multi-wire ionization detectors

through (1.3):

$$x(z) = x_o + \frac{p_{y_o}}{qB_z}\left[\frac{1}{\sin\varphi}\sin\left(\frac{qB_z}{p_z}(z-z_o)-\varphi\right)+1\right], \tag{1.1}$$

$$y(z) = y_o + \frac{p_{x_o}}{qB_z}\left[\frac{1}{\cos\varphi}\cos\left(\frac{qB_z}{p_z}(z-z_o)-\varphi\right)-1\right], \tag{1.2}$$

$$z(z) = z, \tag{1.3}$$

where x_o, y_o, p_{x_o} and p_{y_o} are determined by the initial conditions:

$$x(z_o) = x_o \quad y(z_o) = y_o \quad z(z_o) = z_o$$
$$p_x(z_o) = p_{x_o} \quad p_y(z_o) = p_{y_o} \quad p_z(z) = \text{const},$$

and φ is the angle defined by the initial momentum components as projected on the xy-plane (or the initial angle of trajectory with respect to the x-axis), which can be written as:

$$\tan\varphi = \frac{p_{y_o}}{p_{x_0}}. \tag{1.4}$$

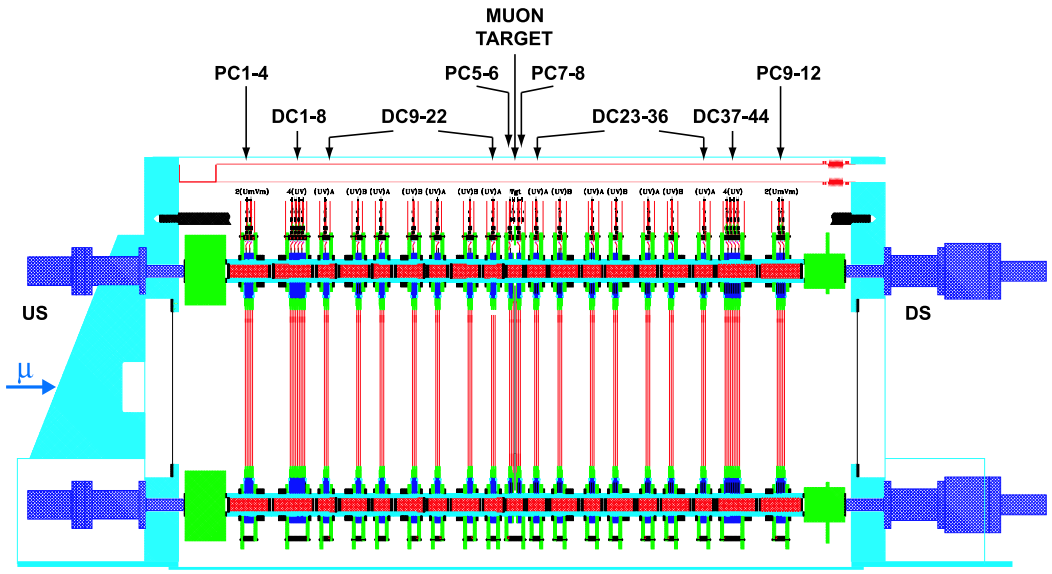

Figure 1.6: $\mathcal{TWIST}$ Spectrometer Side View
Courtesy of TRIUMF and $\mathcal{TWIST}$

The PCs are used for fast timing measurements; they are located at the entrance and exit of both upstream and downstream chambers. PCs contain a "fast" gas (i.e. the produced ions drift back to the cathode relatively quickly), enabling smaller time scale measurements than the DCs. These measurements are needed for obtaining the start and end times of the muon and positron tracks. If no start or end times are available, there could not be a position calculation (this will be illustrated later in the analysis discussion of Chapter 2).

The work that follows is the result of an analysis of the effects created by space charges and dead zones in the PCs closest to the target. So a more detailed understanding of the inner workings of proportional counters is required—such is the subject of the following sections.

1.4 Proportional Counters

A proportional counter is a type of wire chamber, and a wire chamber is a type of radiation detector. These types of detectors are constructed as shown in Figure 1.7, with a plane of wires suspended between two planes of metalic foil which act as cathodes. When a negative voltage is applied to the foils a positive charge is induced on the anodes, creating an electric field similar to the one shown in Figure 1.5. For an infinite anode plane with wires of zero diameter, the equation for the electric potential is given by: [9]

$$V(x,y) = -\frac{CV_o}{4\pi\epsilon} \ln\left[4\left(\sin^2\frac{\pi x}{s} + \sinh^2\frac{\pi y}{s}\right)\right], \tag{1.5}$$

where:

- $V_o \rightarrow$ Applied voltage.
- $\epsilon \rightarrow$ Di-electric constant of gas used to fill the entire space between the two cathodes.
- $s \rightarrow$ Distance between two adjacent wires.
- $L \rightarrow$ Distance between anode wire and cathode planes.
- $d \rightarrow$ Anode wire diameter.
- $C \rightarrow$ Anode-cathode capacitance. Also, if $d \ll s \ll L$ then:

$$C = \frac{2\pi\epsilon}{\frac{\pi L}{s} - \ln\left(\frac{\pi d}{s}\right)}. \tag{1.6}$$

Obviously the assumptions made above are not met in a real wire chamber, but equations (1.5) and (1.6) are good approximations of most cases.

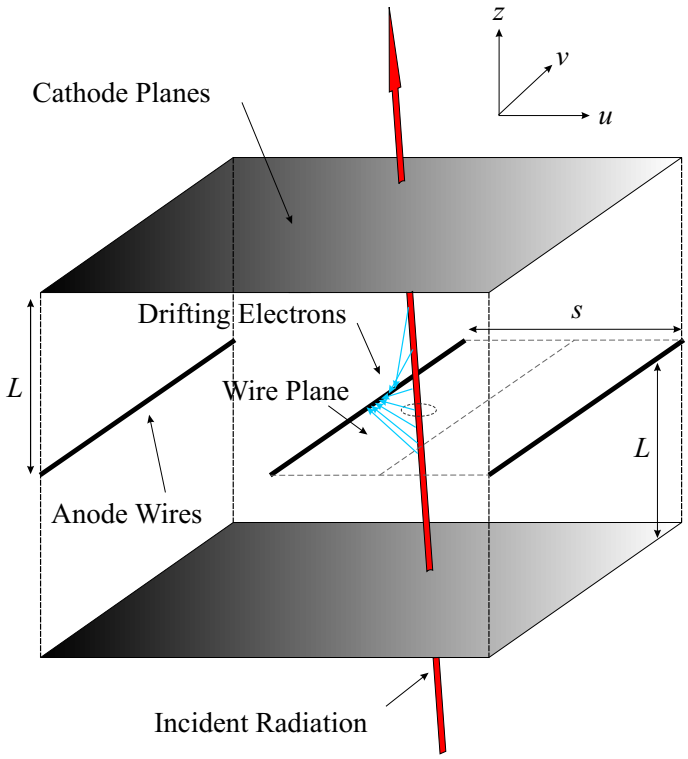

Figure 1.7: Multi-Wire Proportional Chamber

The chamber is filled with a neutral gas (like a noble gas) at constant pressure, such that incident radiation interacts with the gas to create an electron-ion pair. The electron and ion are then accelerated to the anode and cathode respectively. In doing so, both charged particles are subject to random collisions with other gas molecules. It is useful to describe this process in terms of particle drift velocity, v_d, and mobility, u. Recall, from kinetic theory, that the drift velocity is the average velocity attained by a particle subject to random collisions with other gas molecules. In this case, the electron has a higher drift velocity than the positive ion because it is much less massive.

The mobility of a charged particle is defined as:

$$u(x,y) = \frac{v_d}{\left|\vec{E}(x,y)\right|}, \tag{1.7}$$

thus, the electron also moves with greater mobility than the ion. But for positive ions, it can be shown that the drift velocity depends only on the ratio of the electric field strength to the pressure of the system: [9]

$$v_d^{ion} \propto \frac{\left|\vec{E}(x,y)\right|}{P}. \tag{1.8}$$

This implies that, for constant pressure, the mobility for positive ions is a constant.

Once the electron is within a few wire radii of the anode wire, it begins to accelerate more rapidly, giving it enough energy to create another electron-ion pair should it collide with another gas molecule. The electron emitted in this secondary collision does the same thing, and so on, producing an avalanche of electron-ions pairs. This avalanche forms a tear drop shape of positive and negative charges as it moves—with mostly electrons at the head, and positive ions at the tail—as illustrated in Figure 1.9.

Since the electrons move with a greater drift velocity, and thus a greater mobility than the positive ions, they drift relatively quickly to the anode wire. A sharp, negative voltage is induced on the anode wire due this quick electron drift. Once the electrons are collected by the positively charged wire, there is no longer an equal amount of positive and negative charges inside the wire chamber. So the positive ions drift back towards the cathode—again, inducing a negative voltage in the anode wire, but this time less quickly than the electrons and with decreasing amplitude. This is the part of the process that contributes to the tail of the voltage pulse—which is much longer in duration than the rise time, as illustrated in Figure 1.8.

The anode wire is connected to processing electronics called "Time to Digital Converters" (TDCs) which analyze the rise time of the signal pulse relative to some other independent timing fiducial. If the peak voltage of the pulse is greater in amplitude than the voltage threshold of the TDCs, they output a signal which is labeled as an event for later processing. This is the method of "detecting" incident

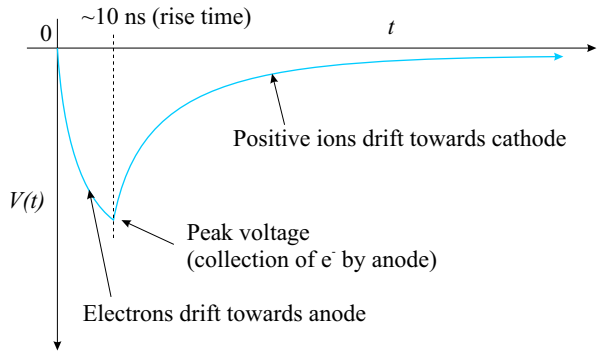

Figure 1.8: Voltage pulse induced by drifting electrons and positive ions inside wire chambers

radiation.

Moreover, proportional counters work in the voltage range of about 200 to 600 volts. [9] In this range, the amount of amplified current produced is proportional to the initial number of electron-ion pairs created. So the signal strength (the total charge, related to the length of duration) is proportional to the energy deposited in the gas by the incident radiation—hence the name "proportional" counter.

Additional information can be found using these detectors. The position at which the radiation passed through the detector can be approximated by the position of the wire which "fired" to produce an observed pulse: $x \pm s/2$. Since the same signal can be produced on either side of the wire, there is a left-right ambiguity. This is taken into account with the $\pm s/2$ term in the position approximation.

However, only *one* position coordinate can be found per wire plane because the wire planes are only sensitive to the direction perpendicular to which the wires run. To get the y-coordinate another plane of wires is needed at a different z-value (preferably close to the location of the chamber measuring the corresponding x-coordinate) with wires running perpendicular to the plane next to it.

1.5 Drift Chambers

Similar to PCs, drift chambers (DCs) use the ionization of neutral gas molecules to detect the position of an event. The difference between DCs from PCs is that their cells are filled with a *slower* gas—that is, the drift velocity of electrons inside the pressurized gas is slow compared to the electron v_d of the gas in PCs.

Although the mechanism for *detecting* radiation is the same, a slightly different method for calculating the position of an event is used with DCs. Suppose the drift velocity of electrons is known as a function of electric field strength for the gas being used, and a timing trigger is also available which gives a very accurate time of initial incidence. Then the position of an event inside the wire chamber can be calculated using:

$$x = \int_{t_o}^{t_f} v_d dt, \tag{1.9}$$

where t_o is the time triggered for initial radiation incidence upon the DC, and t_f is the time detected by the TDCs governed by the rise time of the signal pulse. Typical timing triggers used in this case are scintillation counters because they are capable of very fast timing (i.e. a few nanoseconds).

Since the electron drift velocity is slow relative to that of electrons inside PCs, the time to drift to the anode wire will be greater—thus the uncertainty in the position calculation will be less. The spacing between the cathode and anode wire is also larger, further lengthening the drift time.

But because of the left-right ambiguity, signals from several wires firing along the same incident particle track must be used to resolve the exact trajectory of a particle through the chamber.

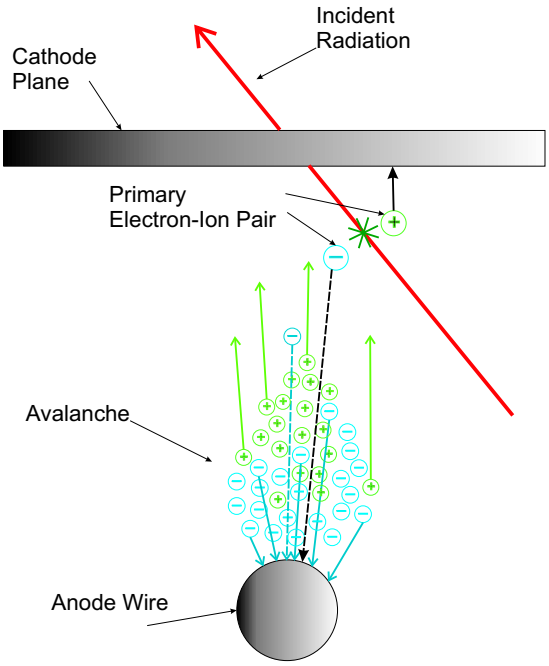

Figure 1.9: Avalanching electrons in a single wire chamber cell

1.6 Space Charges and Dead Zones

With this background understanding of the mechanisms inside PCs, the theory and the importance of space charges and dead zones inside PCs can now be discussed.

When detecting muons in a PC, the muon deposits the most amount of energy in the gas near the end of its track, just before it decays. This relatively large deposit of energy at the end of the track forms many electron-ion pairs, each electron creating its own avalanche. Most of the ions are then created near the anode wire, where they must drift back towards the cathode (this is illustrated in Figure 1.9). Such a large number of localized positive ions is called a *space charge* inside the wire chamber. This space charge has a finite decay time over which the ions either recombine with electrons or drift back to the cathode.

Now, the $\mathcal{TWIST}$ experiment is focussed not only on observing muons decay, but on measuring paths of positrons emitted from each decayed muon relative to that initial muon's path. Suppose the muon decays upstream, emitting a positron back

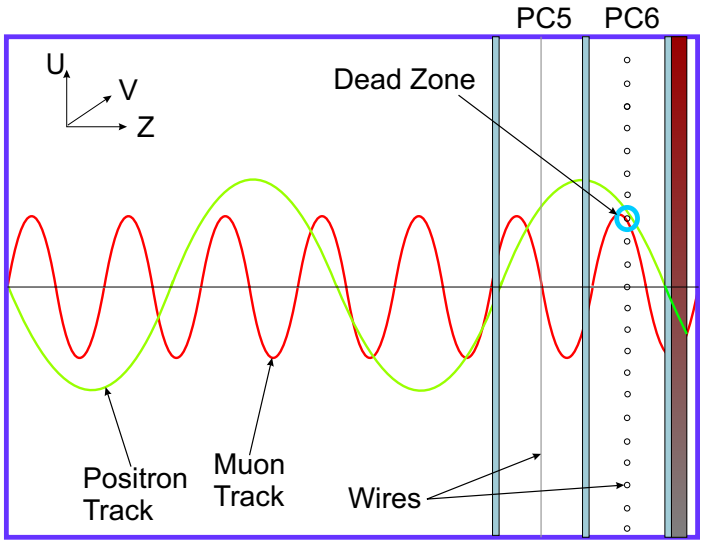

Figure 1.10: Dead zone penetration in PC6 from an upstream muon-decay positron

through the same region the muon already penetrated—thus, back through a region containing the space charge, as illustrated in Figure 1.10. In this case, any additional electron-ion pairs that are formed by the positron either recombine with the high density of positive ions that compose the space charge, or they are redirected away from the anode wire because the electric field has been distorted by the space charge. Without an electron-ion pair specific to that positron, no pulse is formed, and thus no position is recorded in the data for that emitted positron (i.e. the muon would be seen to traverse the PCs and then decay, but no emitted positron would be recorded). This region containing the space charge is what we call the "Dead Zone", since the cells containing the wires act as if they are "dead" (this is illustrated in Figure 1.11).

This study of dead zones is, therefore, done mostly on PC5 and PC6, which are located nearest the muon target in the upstream chamber.

1.7 A Refined Goal

The specific goal of this dead zone study is to answer the following questions:

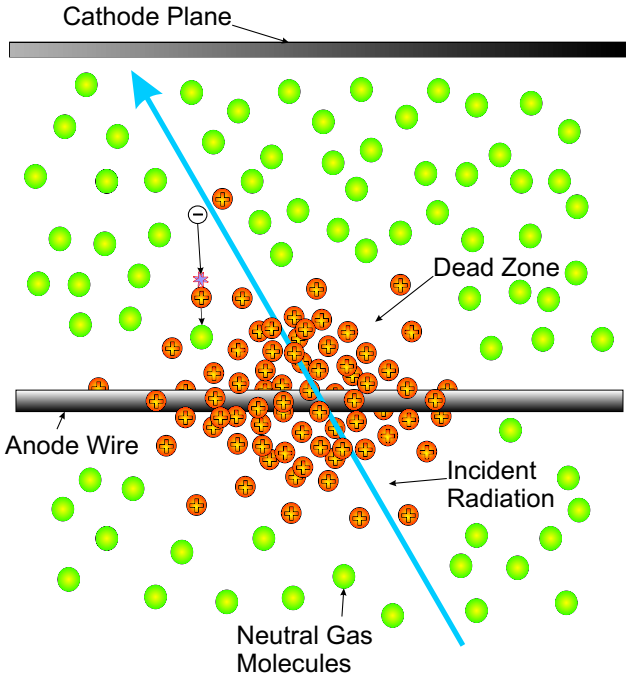

Figure 1.11: Effect of Dead Zone

(1) How large, on average, is the dead zone?

(2) How long does it take, on average, for the dead zone to "heal"?

(3) What is the probability that a positron will go through the dead zone without firing the corresponding wire?

(4) What effect does this dead zone have on the analysis of the Michel parameters? In other words, what is the systematic uncertainty on the measurements of the Michel parameters caused by the dead zone effect?

These questions can be answered through careful inspection of the raw wire chamber data, and with the help of Monte Carlo analysis using GEANT3. The first step in the process was to identify the specific data variables needed to answer these questions; then a computer code was written to fill different histograms (under well-defined "right" conditions) containing the identified useful information.

As illustrated in this thesis, there are a number of checks that can be performed to ensure the analysis and extracted results are reasonable. One such check would be to run the developed analysis program on a set of Monte Carlo "pseudo data" and observe whether or not similar results to the actual raw data are obtained.

The Monte Carlo simulation of the TWIST spectrometer is essential to this study. For example, there is no a priori way of testing how large the dead zone is, or how long it lasts, without implementing specific numbers in the GEANT3 Monte Carlo simulation code of the TWIST experiment. How the GEANT3 simulation code was used to interpret the dead zone analysis of the raw data will be illustrated in Chapter 2.

Chapter 2

Analysis of $\mathcal{TWIST}$ Data

To understand the analysis performed on the raw data one must understand what kind of information is recorded and stored in the $\mathcal{TWIST}$ "event stream" during data acquisition.

$\mathcal{TWIST}$ measures the helical tracks of positive muons and their decay positrons inside a magnetic field by using many dense planes of wire chambers. The source of muons is the M13 beamline, which electromagnetically chooses polarized muons from a source of pion decay. The rate of muon incidence on the $\mathcal{TWIST}$ spectrometer is kept relatively constant at a few hundred μA throughout a measuring period.

A series of electronic counting and timing devices record the events fired at each wire chamber and stores them in binary format on discs for later extraction. The sorting and analyzing of these data is done using various $\mathcal{TWIST}$ software routines.

2.1 $\mathcal{TWIST}$ Software

As in any modern subatomic physics experiment, the $\mathcal{TWIST}$ experiment is extremely dependent on its software to make sense of the information from the detectors stored for every "event". Most of the $\mathcal{TWIST}$ software is custom built, and requires fast computing power and vast memory banks to store both the raw data and the analysis results. In fact, the computing facilities at TRIUMF are insufficient for the jobs $\mathcal{TWIST}$ requires. The experiment has acquired high priority on the WESTGRID computing facility. This organization provides the CPUs for computing and storing data for many outside universities and organizations along the west coast.

There are two main processes through which the raw data must be run in order

to obtain the information needed for this study:

(I) **MOFIA Analysis**

MOFIA is the main analysis code written by the *TWIST* collaboration. It uses the initial binary files that were created in sets during the first two years of data-taking. These files contain all the raw data directly from the electronics connected to the *TWIST* spectrometer.

For each set of data (each containing $\sim 2.5 \times 10^8$ events) there are about 200-300 "runs" (seperate files) that divide up the events. For each run, MOFIA creates a `.root` file that contains histograms of various "raw" recorded quantities, and also of variables that are derived/calculated from the raw data.

TWIST events are catagorized by MOFIA into about 25 different event types. The work done in this thesis only required knowlegde of event type 1, which is defined as:

> **Event Type 1:** Simple Clean
>
> A muon and its decay positron, seperated by more than 1050 ns. No other windows in the event.

The MOFIA analysis also splits events into catagorized time "windows", such that no two events overlap in the same window. This allows access to variables like position and momentum *specific* to each particle in a given event (for example, the μ^+, or the e^+).

For each set analyzed by MOFIA, there are 200-300 output files labeled: `treerun#.root` which need to be summed in order to get useful information (since each individual run has an insufficiently large event sample for good statistical analysis). This is the next step.

(II) **ROOT Tree Summing**

ROOT is a very powerful object oriented physics analysis program that uses the `c++` language as a platform; this program was developed at CERN [1]. *TWIST* uses this software to conveniently store statistical information related to the event-by-event "Ntuple" data in a special ROOT data structure called a "tree".

ROOT trees are similar to directories in that a single tree can contain many types of data structures. There are three main types of data structures used by this experiment in the ROOT trees:

(i) Histograms

(ii) Ntuples

(iii) Leaves

Histograms and Ntuples are well known and used in many areas of physics, but "leaves" are somewhat unique to ROOT. Leaves are basically variables in array form that can be accessed in the same way as arrays or pointers passed as arguments in a function. Leaves can even be histogramed under any logical condition inside the ROOT viewer. [7]

Using a computer code written by members of the *TWIST* group, the `.root` run-files in each analyzed data-set can be summed over all the information in each file, thus reducing the subsequent analysis to requiring only a single `.root` file.

Once this preliminary analysis is completed, any information needed from a given data-set can be extracted from a single file. Moreover, by modifying the tree-summing code, new histograms can be accumulated under very specific (user-defined) criteria. This is the part of the analysis that was done in this study, and is the subject of the next section.

2.2 The Code

The bulk of the dead zone analysis is done by the set of subroutines attached to the end of Blair Jamieson's ($\mathcal{TWIST}$ collaborator) `HTree` (tree-summing) analysis code. The following is a list and description of the code implemented in the version of `HTree` specific to this dead zone analysis.

(1) `HTree.C` and `HTree.h`

These are the implementation and header files of the main `HTree` analysis code. The last few lines contain the definitions of the subroutines written to perform the dead zone analysis, which are called:

(i) `Deadzone()`

(ii) `DZComputHistos()`

(iii) `DZ_ErrorBars()`

(iv) `TH2D_Divide()`

(v) `TestTrackToZ()`

(2) `processhelixtrees`

This is the executable that performs `HTree` analysis.

(3) `trackswim.cpp` and `trackswim.h`

This code is just like it sounds, it "trackswims" a particle of charge q, from an initial position (u, v, z) with momentum initial (p_u, p_v, p_z), through a uniform or non-uniform $\vec{B}$-field to a requested final z-position (`ENDZ`). It then outputs the new coordinates (u, v, `ENDZ`) and the momentum at the end location.

(4) `magnet.cpp` and `magnet.h`

This code calculates the $\vec{B}$-field data: (B_u, B_v, B_z) at all neccessary (u, v, z) for the uniform or non-uniform cases, with the help of the internationally standardized magnetic field mapping program OPERA (which produces a map of the $\vec{B}$-fields within the $\mathcal{TWIST}$ spectrometer).

As discussed above, once the raw data (or Monte Carlo pseudo-data) sets are run through the main analysis software MOFIA, the information is output into `.root` files in the form: `treerun#.root`. The "Deadzone" code runs while the trees are being summed, and outputs histograms that contain useful information about the dead zone (this will be shown in later sections).

2.3 The Geometry

The geometry of the spectrometer is crucial to understanding how to tackle this dead zone problem. As mentioned before, there are two types of wire chambers in the spectrometer: drift chambers and proportional counters. For this analysis, specific knowledge of the location of each of these chambers relative to the target stop (at $z = 0$) is needed. The following subsections provide a good description of this geometry. Since the $\mathcal{TWIST}$ spectrometer is designed such that incident muons decay in the target, there are very few polarized muon decay vertices in the downstream half of the detector (i.e. $z > 0$). Since the dead zone problem arises when an emitted positron travels back through the same wire chamber cell where the parent muon had previously traversed, dead zones are only significant in the *upstream* half of the spectrometer (since this is the volume that muons are guaranteed to penetrate). Thus, the geometery information needed here is only that of the upstream (US) half (i.e. $z < 0$) of the spectrometer.

2.3.1 US Drift Chambers

Geometry data for the US drift chambers is given in Table 2.1. To interpret the information in Table 2.1 (and Table 2.2), there are a few parameters which need an explanation:

- The "Global Plane" numbers are simply plane numbers defined as the sequential order in which the muon would hit the planes if it went straight through the spectrometer.
- Z is the distance, in cm, from the target stop.
- The "Rotation" is the angle relative to horizontal at which the wire chambers are rotated.
- The "Instrumented Wires/Plane" is the number of wires that are actually hooked up to counting electronics. There are the same number of wires per plane in all DCs and PCs. The wires that are not instrumented can still cause multiple scattering of the muon and positron. There are 80 wires per plane in any DC, with a wire spacing of $s = 0.4$ cm.
- The "Plane Type" depends on the angle of rotation. If the plane type is V, then the wires run along the U-direction and measure the v-coordinate of the tracks. If the plane type is U, then the wires run along the V-direction and measure the u-coordinate of the tracks.

2.3.2 US Proportional Counters

Geometry data for the US proportional counters is given in Table 2.2. Each wire chamber contains one plane of wires, and each plane contains 160 wires (except the last two planes in the US chamber, which only have 48 of those wires instrumented). The

Global Plane #	Z (cm)	Rotation (°)	Instrumented Wires/Plane	Plane Type
5	−49.7929	−45.0	48	V
6	−49.3929	45.0	48	U
7	−48.9929	−45.0	48	V
8	−48.5929	45.0	48	U
9	−48.1929	45.0	48	U
10	−47.7929	−45.0	48	V
11	−47.3929	45.0	80	U
12	−46.9929	−45.0	80	V
13	−42.1933	45.0	80	U
14	−41.7933	−45.0	80	V
15	−34.9948	45.0	80	U
16	−34.5948	−45.0	80	V
17	−29.7950	45.0	80	U
18	−29.3950	−45.0	80	V
19	−22.5968	45.0	80	U
20	−22.1968	−45.0	80	V
21	−17.3975	45.0	80	U
22	−16.9975	−45.0	80	V
23	−10.1993	45.0	80	U
24	−9.7993	−45.0	80	V
25	−4.9997	45.0	80	U
26	−4.5997	−45.0	80	V

Table 2.1: Geometry Data for Upstream DCs

wire spacing is $s = 0.2$ cm for all PCs and $s = 0.4$ cm for all DCs. All instrumented wires are located in the central region of the wire chambers, encompassing the muon beam spot.

Global Plane #	z(cm)	Rotation (°)	Instrumented Wires / plane	Plane Type
1	−59.79	45.0	160	U
2	−59.39	−45.0	160	V
3	−58.99	45.0	160	U
4	−58.59	−45.0	160	V
27	−0.6	135.0	48	V
28	−0.2	−135.0	48	U

Table 2.2: Geometry Data for Upstream PCs

2.4 The Algorithm

In order to extract information about the dead zone in a particular wire chamber, the following algorithm is invoked:

For each event in a `treerun#.root` file, only events satisfying the following four criteria (or "tests") were selected for the analysis:

(i) Event Type = 1

This type of event can be categorized as "Simple, Clean".

(ii) Window Type = 2

Events categorized into this timing window correspond to positrons that were emitted in the upstream direction from a muon decay vertex in the target.

(iii) $p_z \geq p_u$

where p_z is the momentum of the emitted positron along the z-direction, and p_u is the momentum of the emitted positron along the u-direction.

(iv) $\left|\vec{P}_{tot}\right| \geq 20$ MeV

where: $\left|\vec{P}_{tot}\right| \equiv \sqrt{p_u^2 + p_v^2 + p_z^2}$ is the magnitude of the total momentum vector for the emitted decay positron.

For events satisfying these criteria, the routine then finds the last (u, v) coordinates of the muon before it decays. This is done by requiring that the last v-plane hit is equivalent to the integer variable `pvlast_anal`, and the last u-plane hit is equivalent to the integer variable `pulast_anal`. The (u, v) coordinates give an approximate location of the dead zone, since it represents where the muon was last "detected" in the last two chambers before the target.

Next, the routine checks to see if the upstream decay positron went back through the dead zone. If it did, then the (u, v) coordinates recorded for the positron in the

data may or may not actually be from the planes last hit by the muon. If the wire was dead when the positron passed by it, there would be no recorded TDC signal from that particular wire. Thus, for such events, the positron's (u, v) coordinates in the data trees cannot be used.

Then, the last recorded position and momentum of the decay positron, (u, v, z) and (p_u, p_v, p_z), are obtained directly from the trees in order to reconstruct its track back to $z =$ `zpulast_anal` (the z-coordinate of `pulast_anal`, the last u-plane where the muon was detected). This must be done in order to find the number of decay positrons that "penetrate" the dead zone in the PC u-plane `pulast_anal`, compared to the number that were actually observed to "fire" a wire in that region. If the coordinates from this tracking are within a certain tolerance of the approximate location of the dead zone (i.e. the calculated coordinates of the positron are "close enough" to the last recorded coordinates of the muon: $|u_{e^+} - u_{\mu^+}| \leq$ tolerance), this event is labeled as "penetrating" the dead zone and histogrammed.

Finally, if the last recorded (u, v) coordinates for the decay positron satisfy this same tolerance criteria, *and* the last recorded wire plane for the decay positron is the same as that recorded for the muon, then this event is labeled (and histogrammed) as "firing" a wire in the dead zone. Note that the tolerances used for these labelings are:

- tolerance = 0.098 cm **for PCs**
- tolerance = 0.198 cm **for DCs**

The values for the tolerance were chosen, in both cases, based on the geometry of the wire chambers. Remember that the wire spacing for PCs is $s = 0.2$ cm, so the distance between a wire and the next cell is $s/2 = 0.1$ cm. Similarly, $s/2 = 0.2$ cm in any DC. The tolerance is chosen such that the decay positrons are allowed to come very close to the boundary between adjacent chamber cells (up to 0.002 cm from the

cell boundary), but are not allowed to cross the boundary. This guarantees that decay positron events from adjacent cells are not counted. Since dead zones are thought to be localized to a single cell, a more accurate count of dead zone penetrating positrons is achieved.

2.5 The Tests

In order to determine whether or not the analysis code is working in a reasonable way, tests were performed as outlined in the following four subsections.

2.5.1 Trackswimming Test

If the last u-plane hit was `pulast_anal`, and the last v-plane hit was `pvlast_anal`, then it is possible to compare the recorded data coordinates to the results of the trackswimming calculation for the decay positron. Histograms of the following values were accumulated:

(1) Histogram: $(u_{fit} - u_{data})$

where u_{fit} is the u-coordinate of the positron as a result of trackswimming back to `pulast_anal`, and u_{data} is the u-coordinate of the positron recorded in data at `pulast_anal`.

(2) Histogram: $(v_{fit} - v_{data})$

where v_{fit} is the v-coordinate of the positron as a result of trackswimming back to `pvlast_anal`, and v_{data} is the v-coordinate of the positron recorded in data at `pvlast_anal`.

This test proved to be very useful. By inspecting the histograms for the u and v-coordinates seperately, an evaluation can be made of whether or not the trackswimming code is working properly. If both histograms show a sharp peak around

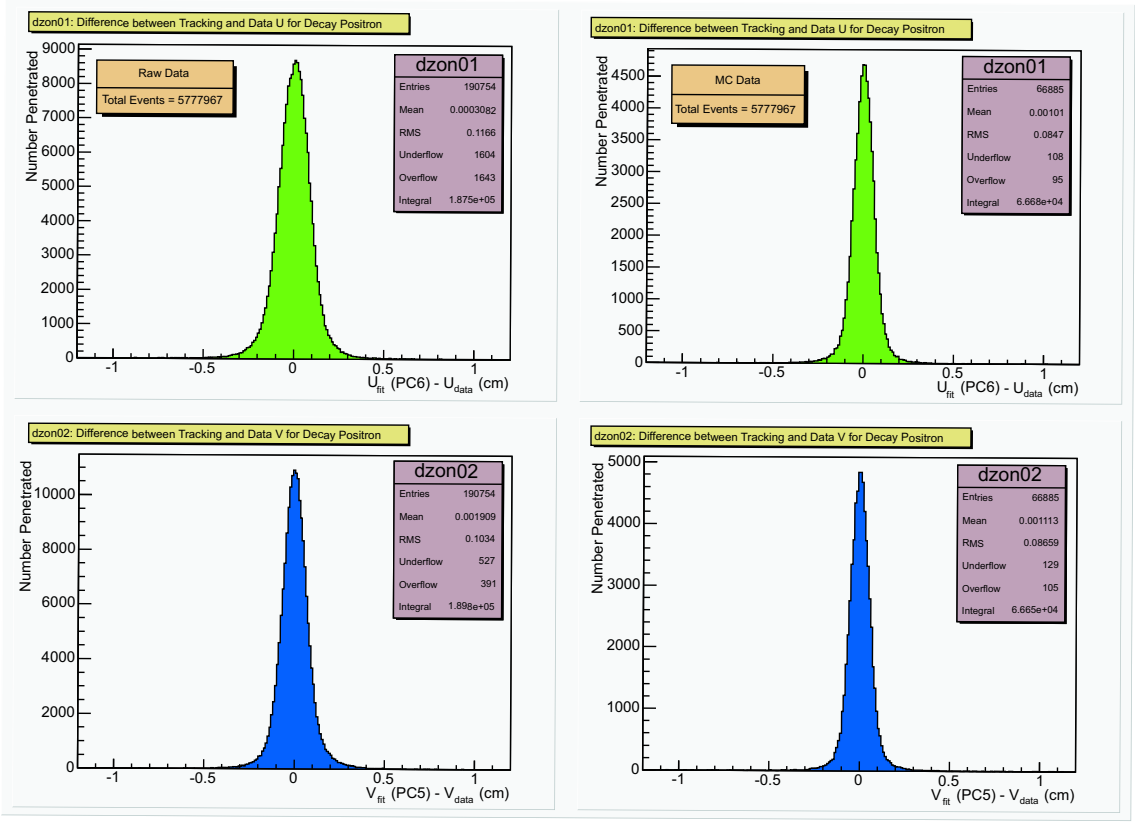

Figure 2.1: Trackswimming test for both raw data and Monte Carlo pseudo-data

zero then the trackswimming calculation is consistent (on average) with the data. These histograms were generated for both raw data (RD) and Monte Carlo (MC) pseudo-data to compare the results; both are shown in Figure 2.1. In fact, this test showed that PC6 was misaligned in the MOFIA analysis by a small amount (relative to where it was thought to be located *physically* inside the spectrometer). This has now been accounted for in the analysis code by artificially shifting all the relavent u-coordinates by a small constant ($u_{shift} = 0.04678$ cm).

Notice in Figure 2.1 that the RMS of the distribution in RD is larger than that for the MC by about 38% in the u-direction, and about 17% in the v-direction. This is evidence that the MC does not *completely* reproduce the tracks of muons and decay positrons that occur inside the spectrometer. It's not a big surprise that the trackswimming results agree more closely with the MC than the RD. Both the track-

swimming and MC are computer generated and neither perfectly represent reality because not all physical processes, nor experimental uncertainties, are fully accounted for. For example, the multiple scattering of charged particles that goes on inside the spectrometer is a very complex process (with scattering of the muons off of the chamber gases, the entrance/exit walls and windows of the chamber, etc.—all serving to slightly alter the muon's direction). In fact, for muons the multiple scattering is so complicated that $\mathcal{TWIST}$ completely avoids fitting muon tracks because they are rarely smooth. The MC simulation is simply a good *approximation* of physical reality, so exact results are not expected—however, close results, such as those illustrated in Figure 2.1, *are* expected.

2.5.2 Muon Beam Spot Test

This is a simple test that confirms whether or not the muon beam spot from the M13 beamline is prepared and aligned properly. This test is illustrated in Figure 2.2, which shows two things:

(1) A projection of the beam spot on the u-axis of PC6 in terms of wire number. The wire number is defined as an ordered integer corresponding to the i^{th} instrumented wire, ranging from negative to positive u, with $u = 0$ being half-way between wires 80 and 81. For example, wire number 1 represents the wire at coordinate: $u = -(80.5)s$, where $s = 0.2$ cm is the wire spacing in PC chambers.

(2) A 2D projection of the beam spot contour plot using u-coordinates from PC6 and v-coordinates from PC5.

The effect wire chambers have on the event coordinates is now clear. The wires make the event coordinates discrete, as opposed to continuous. On the beam spot, high numbers of counts occur only where two wires cross (as illustrated by the color

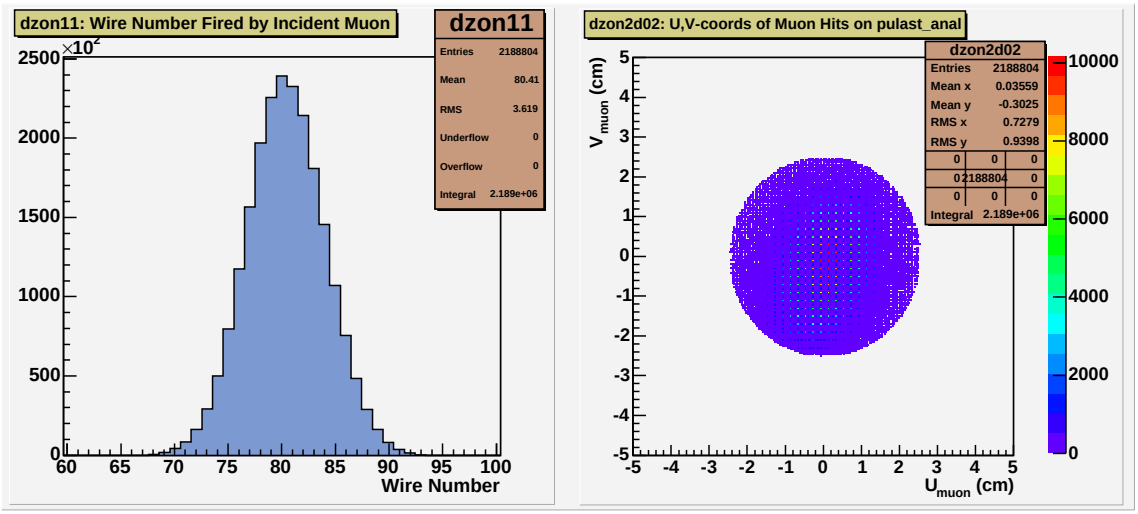

Figure 2.2: Muon beam spot test (dzon11 & dzon2d02), taken from RD set2/anal9

coded contour plot). However, some counts occur in between wires. This is due to the weighted average performed in the analysis of the wire chamber hits when more than one wire fires for the same event.

If there is something out of the ordinary in the code, inspecting the shape of the beam spot may reveal it. The mean value of counts along the v-direction in the beam spot is slightly off center, with a value of -0.3025 cm. It is well known that the muon beam spot is not perfectly symmetric, and the distribution shown in Figure 2.2 agrees with the actual beam spot.

The circular asymmetry of the muon beam spot should cause an asymmetry in the decay positron hits along the v-direction.

2.5.3 Dead Zone Test using Wire Numbers

This is a test that shows indirect evidence of the dead zone. On the left hand side of Figure 2.3 is a stack of two histograms. The larger, green histogram is the number of positrons *penetrating* the dead zone while the smaller, blue histogram is the number of positrons that caused a wire to *fire* in the dead zone. Both are in terms of the wire

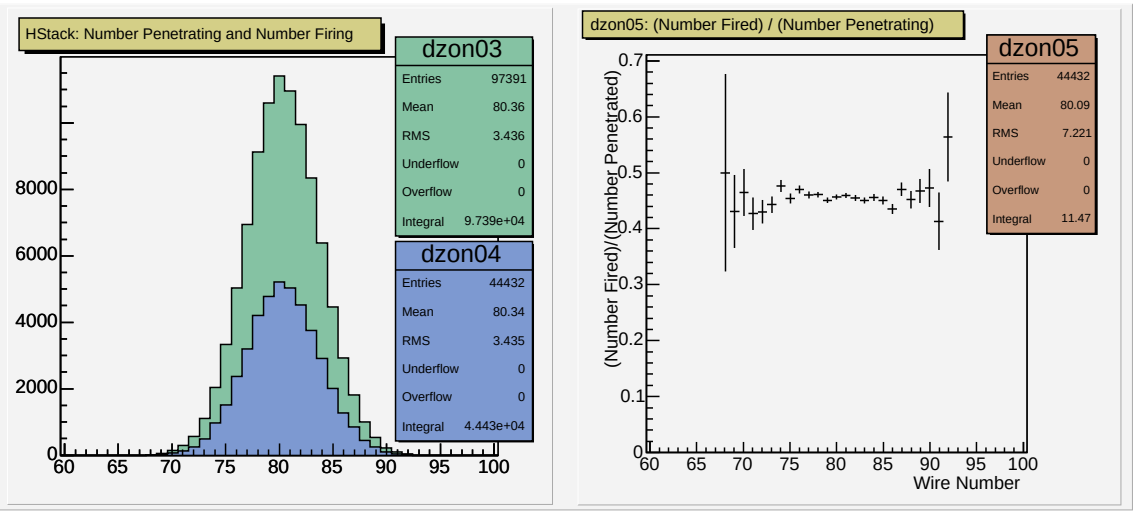

Figure 2.3: Dead zone test using wire numbers (dzon03/dzon04 & dzon05), taken from RD set2/anal9

number in PC6.

On the right hand side of Figure 2.3 is the ratio: (number firing) / (number penetrating), histogrammed as a function of wire number in PC6. The constant value of this histogram is a measure of the probability that a positron will fire a wire when it penetrates the dead zone. According to the figure, about 45% of the positrons will fire a wire, while the rest don't fire wires in the dead zone at all. The error bars plotted in Figure 2.3 were calculated using:

$$\sigma = \frac{\sqrt{N\left(1-\frac{N}{T}\right)}}{T} \tag{2.1}$$

where:

- $N \rightarrow$ Number of positrons firing wires inside the dead zone
- $T \rightarrow$ Number of positrons penetrating the dead zone

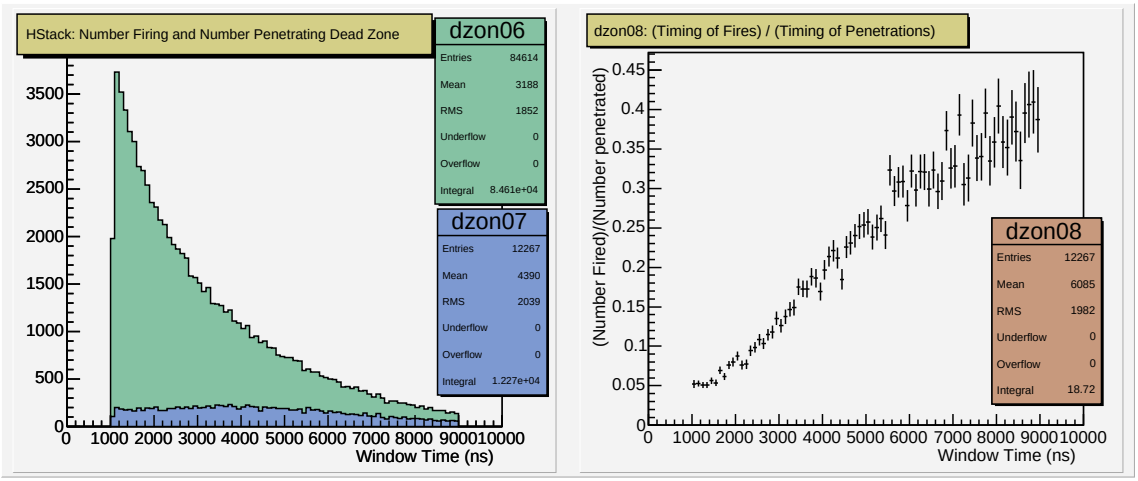

Figure 2.4: Dead zone test using window times (dzon06/dzon07 & dzon08), taken from RD set2/anal9

2.5.4 Dead Zone Test using Window Times

Similar to Figure 2.3, Figure 2.4 contains the same histogram stack, except now shown in terms of window time (in units of ns). The number penetrating the dead zone has an exponential decay rate characteristic of the muon lifetime: $\tau_\mu = 2197.03$ ns. [5]

Also, the same ratio is plotted on the right hand side, which is a measure of the probability for a positron to fire a wire when penetrating the dead zone. This probability increases with time, which makes sense because the muon has less probability of creating space charges as its decay time is reached. That is, less and less muons are present in the spectrometer as the window time increases because they have a lifetime much shorter than the window time duration.

2.6 Direct Observation of the Dead Zone: The Dead Zone Histogram

The most important histograms in this analysis which allow for observation and characterization of the dead zone are shown in Figure 2.5. In order to illustrate

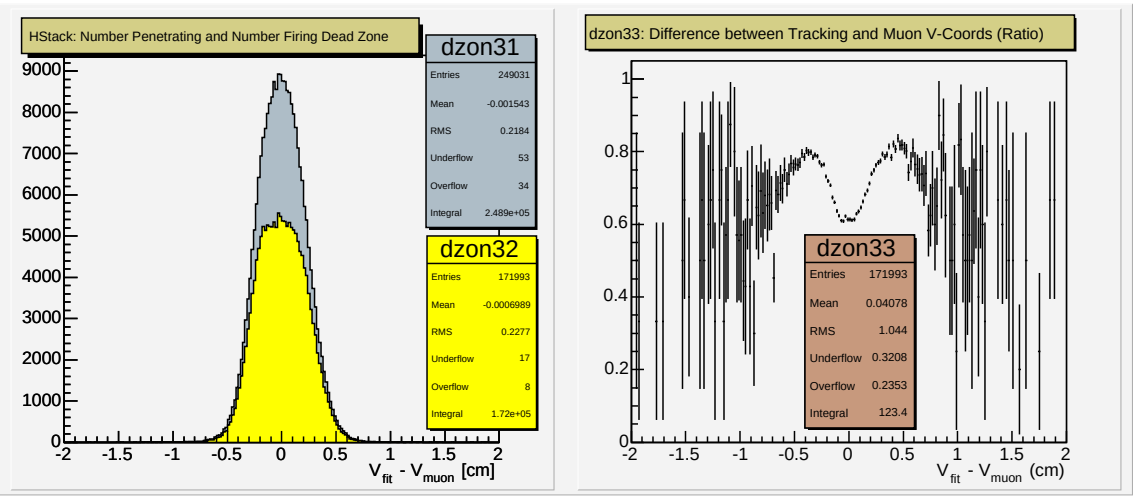

Figure 2.5: The number of positrons penetrating and the number firing a wire in PC6 plotted as a function of $v_{fit} - v_{muon}$

evidence of the dead zone, a histogram was first made with the number of positrons *penetrating* the dead zone as a function of $(v_{fit} - v_{muon})$, where:

- $v_{fit} \rightarrow v$-coordinate (measuring the direction *along* the wires in PC6) from trackswimming of the positron.
- $v_{muon} \rightarrow v$-coordinate (measuring the direction *along* the wires in PC6) of the muon recorded in data.

With these definitions, when the muon and the positron pass near the same v-coordinate along a particular wire: $v_{fit} - v_{muon} \approx 0$.

Next, the number of positrons that actually *fired* a dead zone wire was histogrammed as a function of the same variable. Once these two histograms were made, it is possible to divide one by the other to form the ratio histogram: (Number Firing) / (Number Penetrating), with the correct error bars (Equation 2.1). All three of these histograms are shown in Figure 2.5: the number of positrons penetrating the dead zone is shown in grey on the left, the number of positrons firing a wire in the dead zone is shown in yellow on the left, and the ratio histogram is on the right.

Notice the significant "well" occuring around $v_{fit} - v_{muon} = 0$. This shows strong evidence of the dead zone in PC6. The "well" occurs around zero because this is where the muon and positron pass through the same region along the wire. If many positrons penetrate this region, but a significantly smaller number of them actually fire that wire, then the ratio of the two will be less than one. The ratio histogram indeed shows a marked decrease in the ratio as $(v_{fit} - v_{muon})$ approaches zero, thus producing a well-like structure. The area inside this well contains information about the average length along the wire that is "dead".

Next, to investigate the time-dependent "healing" property of the dead zone, a 2D histogram was constructed with the ratio values for all the available window times: $1050 \leq t_{win} \leq 9000$ ns. [1] Plotting this as a `lego2` plot in ROOT gives the result shown in Figure 2.6. [7] This 2D plot shows information similar to Figure 2.5— in fact if this plot is integrated over time, the result is that of Figure 2.5. It is clear that the "well" changes as a function of time. The well (which represents the dead zone) becomes less and less defined as time increases, smoothing out while the ratio of the entire region approaches one.

The next step is to closely analyze these two "dead zone" plots in order extract useful information regarding the character of the dead zone. The time-dependence of the well has some underlying relation to the "healing" time of the dead zone and the spatial extent of the well has a relation to the length of the dead zone. This analysis is the subject of the next section.

2.7 The Fitting

Information about the dead zone—specifically the average length that is "dead" along a wire (L_{dead}) and the average lifetime needed for the dead zone to heal (τ_h)—can

[1] This operation required the use of my subroutine "T2DHDivide", which divides one 2D histogram by another. There is not yet a function in ROOT which performs this operation.

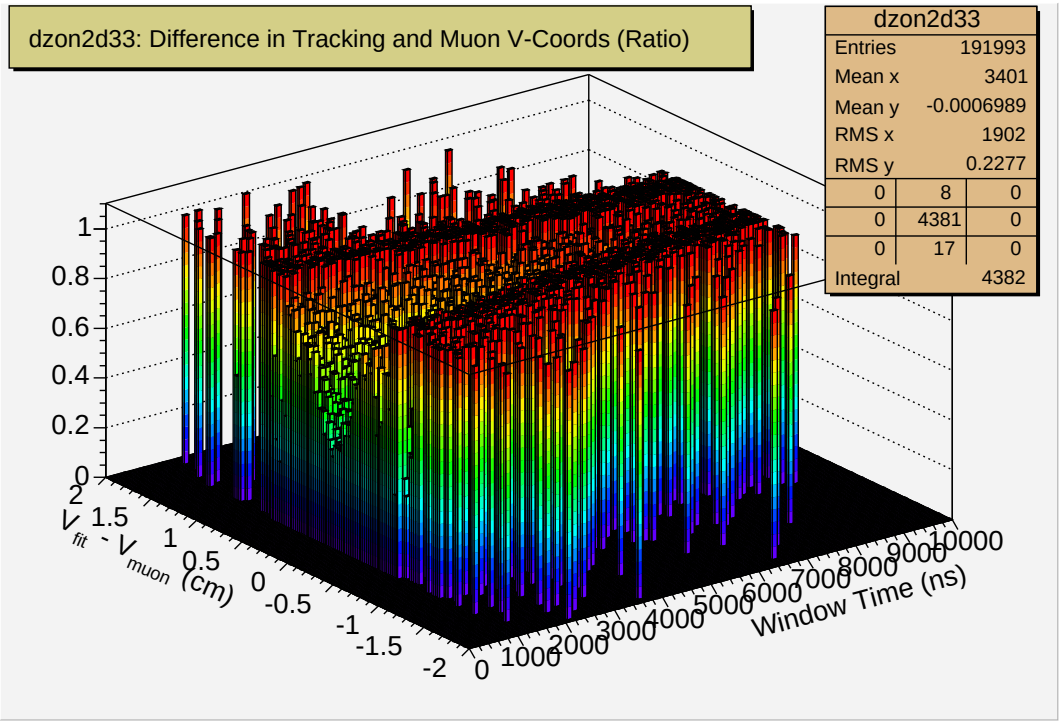

Figure 2.6: The "dead zone" histogram for PC6: the ratio of (number fired / number penetrated) shown as a function of $v_{fit} - v_{muon}$ and window time.

be extracted from the dead zone plot in Figure 2.6. To extract this information, the data were fit using the standard MINUIT non-linear least squares fitting algorithm (supported by ROOT) with a predefined function. A short ROOT-macro was written to fit the dead zone histogram in Figure 2.6 with the following function:

$$Z(x,t) = -\frac{A_o}{\sqrt{2\pi}\sigma}\exp\left[-\frac{(x-\alpha)^2}{2\sigma^2} - \frac{t}{\tau_h}\right] + \xi \tag{2.2}$$

where:

- $Z \rightarrow$ the ratio of (number firing / number penetrating), as plotted in Figure 2.6.
- $x \rightarrow (v_{fit} - v_{muon})$
- $t \rightarrow t_{window}$ (the window time)
- $A_o \rightarrow$ parameter; Gaussian amplitude

- $\tau_h \rightarrow$ parameter; Dead zone healing time
- $\alpha \rightarrow$ parameter; Offset from $x = 0$
- $\sigma \rightarrow$ parameter; Gaussian RMS
- $\xi \rightarrow$ parameter; Offset from $Z = 0$

(the motivation for using this function will be explained later).

The parameter A_o in this function is related to the dead length L_{dead}. This relation can be found by studying the Monte Carlo simulation of the experiment. Suppose, in the simulation, a dead zone is implemented based on knowledge of its effects. Specification of the size and duration time of the dead zone in the simulation requires input parameters: L_{dead} and τ_h. Then a large number of events are accumulated using the simulation code, and they are analyzed with the "Deadzone" code. So the question becomes: how can the input parameters (L_{dead} and τ_h) be found from the analysis results?

In the Monte Carlo simulation code, the dead zone is approximately represented by a square well similar to the ratio histogram shown in Figure 2.5. But since the experiment is measured with limited resolution, measuring the simulated data with the "Deadzone" analysis code gives a "smeared" result, as shown in Figure 2.5. This "smearing" of data from the input stream to the ouput stream can be described by convolution theory. Recall the definition of a convolution as given by: [12]

$$C(x) \equiv s * g = \int_{-\infty}^{\infty} s(t)g(x-t)dt. \tag{2.3}$$

If $s(x)$ is the original function (square well), and $g(x)$ is the smearing function (normalized Gaussian), then the convoluted function is $C(x)$.

Let $s(x)$ and $g(x)$ be defined as follows:

$$s(x) = \begin{cases} \xi & \text{if } |x| > L/2 \\ 0 & \text{if } |x| \leq L/2 \end{cases}, \tag{2.4}$$

$$g(x) = \frac{A}{\sqrt{2\pi}\sigma} \exp\left(\frac{-x^2}{2\sigma^2}\right). \tag{2.5}$$

Then it can be shown that the convolution of $s(x)$ with $g(x)$ is:

$$C(x) = \frac{\xi A}{2}\left[\text{erfc}\left(\frac{x + L/2}{\sqrt{2}\sigma}\right) - \text{erfc}\left(\frac{x - L/2}{\sqrt{2}\sigma}\right) + 2\right] \tag{2.6}$$

$$= -\frac{\xi A}{\sqrt{\pi}} \int_a^b e^{-t^2} dt + \xi A, \tag{2.7}$$

where:

$$a = \frac{x - L/2}{\sqrt{2}\sigma}, \qquad b = \frac{x + L/2}{\sqrt{2}\sigma},$$

and $\text{erfc}(x)$ is the complementary error function, defined by: [8]

$$\text{erfc}(x) \equiv 1 - \text{erf}(x) = \frac{2}{\sqrt{\pi}} \int_x^\infty e^{-t^2} dt. \tag{2.8}$$

It is now clear that this particular convolution is quite complicated, and cannot be reduced from its integral form; but under certain conditions it can be approximated by a Gaussian with a negative amplitude. As shown in Figure 2.7, there are two extremes to the function in Equation (2.7): one is when $\sigma \ll L$, the other is when $\sigma \gg L$.

For the first case: $\sigma \ll L$ (shown on the top plot of Figure 2.7), the curve shape is dominated by the two error functions *individually*; that is, they overlap in regions of x where their values are small. Thus, the overall convolution curve is *not* dominated by the sum of the error functions.

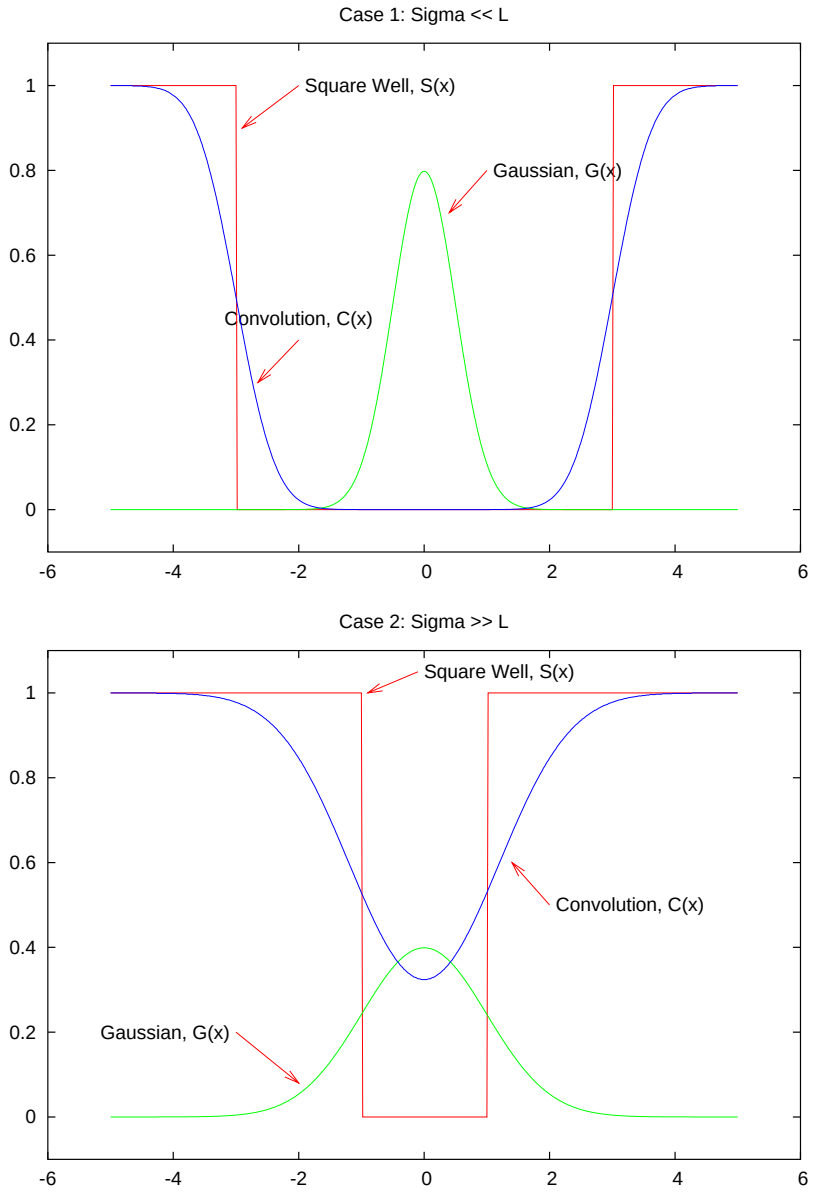

Figure 2.7: The two extreme cases of the convolution $C(x)$

However, for the second case: $\sigma \gg L$ (shown on the bottom plot of Figure 2.7), the convoluted curve shape *is* dominated by the sum of the two error functions. The result is something that can be approximated by a Gaussian with a negative amplitude. This is the case of interest. [2]

[2]This data could be fit by an error function, but it is considerably simpler to model it with a normalized Gaussian function as described.

Convolutions have a useful property: the area under the curve of the convolved function, $s(x)$, is conserved in the convolution, $C(x)$. If the area under the curve of the square well $s(x)$ is equal to that of the convolution $C(x)$, then the area *inside* the well of $s(x)$ is also equal to the area *inside* the well of $C(x)$, which is no longer square and impossible to integrate analytically. But if $C(x)$ is approximated by a Gaussian it becomes rather simple to find the area inside the well.

The relation between the input parameter L_{dead} and the amplitude calculated in the analysis, A_o, follows. The conservation of area property of convolutions is implemented by equating the following two expressions:

$$\int_{-\infty}^{\infty} \hat{s}(x)dx = \xi L_{dead}, \tag{2.9}$$

$$\int_{-\infty}^{\infty} \hat{C}(x)dx \approx \int_{-\infty}^{\infty} \frac{A_o}{\sqrt{2\pi}\sigma} \exp\left(-\frac{x^2}{2\sigma^2}\right) dx = A_o. \tag{2.10}$$

where:

$$\hat{s}(x) = \xi - s(x), \qquad \hat{C}(x) = \xi - C(x).$$

When Equations (2.9) and (2.10) are set equal to each other, a very simple relation between the dead length L_{dead} and the amplitude of the convolution A_o is found:

$$L_{dead} = \frac{A_o}{\xi}. \tag{2.11}$$

This result can be implemented into the fitting function, from which the dead length and an associated error can be calculated directly. The result is:

$$Z(x,t) = -\frac{\xi L_{dead}}{\sqrt{2\pi}\sigma} \exp\left[-\frac{(x-\alpha)^2}{2\sigma^2} - \frac{t}{\tau_h}\right] + \xi. \tag{2.12}$$

The motivation for using this function now becomes quite evident: a normalized Gaussian with a negative amplitude along the x-direction models the dead zone

"well", and it is assumed that the well *heals* (or decays) exponentially—hence, the e^{-t/τ_h} factor. The remaining task is to actually fit the "dead zone" histogram shown in Figure 2.6, and observe how well this empirically derived function models the data. Before discussing this final observation of the data, the next section focuses on modeling a set of Monte Carlo pseudo-data as a test of appropriateness for the interpretation of the fits as given.

2.8 The Monte Carlo Fit

In order to prove the relation given in Equation (2.11) between L_{dead} and the fit parameters, A_o and ξ, a small test set of Monte Carlo pseudo-data was constructed using the experiment simulation code. This set was constructed with a "simulated" dead zone inside PC6. The simulated dead zone requires two input parameters that describe its average size (L_{dead}^{MC}) and its average length of duration (τ_h^{MC}). The goal of fitting this particular MC set is to compare the "measured" dead length and healing time—extracted as described above, by fitting the accumulated "dead zone" histogram with the function in Equation (2.6)—with those input into the simulation. If the measured dead length (L_{dead}^{fit}) and healing time (τ_h^{fit}) are within approximately one standard deviation of the input parameters, then the dead zone model agrees with the simulated dead zone and the fit procedure is deemed appropriate for "measuring" L_{dead} and τ_h. If not, then more work needs to be done to establish the proper link between model and simulation.

The input parameters for the Monte Carlo simulation are:

$$L_{dead}^{MC} = 0.48 \text{ cm}, \qquad \tau_h^{MC} = 2444 \text{ ns}. \tag{2.13}$$

The results of the non-linear least squares fit to this particular histogram using Equa-

tion (2.12) are:

$$L_{dead}^{fit} = (0.5109 \pm 0.0253) \text{ cm}, \qquad \tau_h^{fit} = (1731 \pm 115) \text{ ns}. \tag{2.14}$$

These results show that the input parameter L_{dead}^{MC} is within $1.22\sigma_L$ (which is approximately $1\sigma_L$) of the fit result L_{dead}^{fit}, where $\sigma_L = 0.0253$ cm. Therefore the fit is in agreement with the input parameters.

However, for the input parameter τ_h^{MC}, the value is not within $\sim 1\sigma_\tau$. It differs from the fit value, τ_h^{fit}, by approximately $6\sigma_\tau$, where $\sigma_\tau = 115$ ns. This indicates that the fit does not agree with the input value τ_h^{MC}.

The number of events in the test simulation was on the order of a few 10^4. This amount of statistics is not sufficient to give an accurate calculation of the healing time for reasons that will be explained in §3.2. Ultimately, low statistics will result in an underestimate of τ_h. An estimate of the healing time larger than $\tau_h = 1731$ ns is needed to agree with the input parameters, and since this is achieved with a larger number of statistics, no conclusion about the healing time calculation can be be drawn from this test set of Monte Carlo pseudo data.

Chapter 3

Results

Using the "Deadzone" analysis code on PC5 and PC6 with 2×10^7 events from set2/anal9, the results obtained from the algorithm outlined in §2.7 are shown in Tables 3.1 and 3.2, respectively. As an illustration, Figure 3.1 shows the fit function

Parameter	Value		Error	
L_{dead}	0.2520	cm	± 0.0101	cm
τ_h	1799	ns	± 70	ns
α	0.0200	cm	± 0.0021	cm
σ	0.1100	cm	± 0.0021	cm
B	0.8855		± 0.0012	
χ^2	ndf		χ^2/ndf	
5254	5897		0.8910	

Table 3.1: Fit Results for the Dead Zone in PC5

Parameter	Value		Error	
L_{dead}	0.4297	cm	± 0.0039	cm
τ_h	2521	ns	± 31	ns
α	−0.0029	cm	± 0.0011	cm
σ	0.1968	cm	± 0.0018	cm
B	0.8576		± 0.0016	
χ^2	ndf		χ^2/ndf	
7101	5771		1.232	

Table 3.2: Fit Results for the Dead Zone in PC6

plotted using the parameters in Table 3.2.

The reduced chi-squareds (ratio of χ^2 over the number of degrees of freedom, ndf) are close to one; this is an indication that both fits (to the dead zones in PC5 and PC6) were done reasonably well.

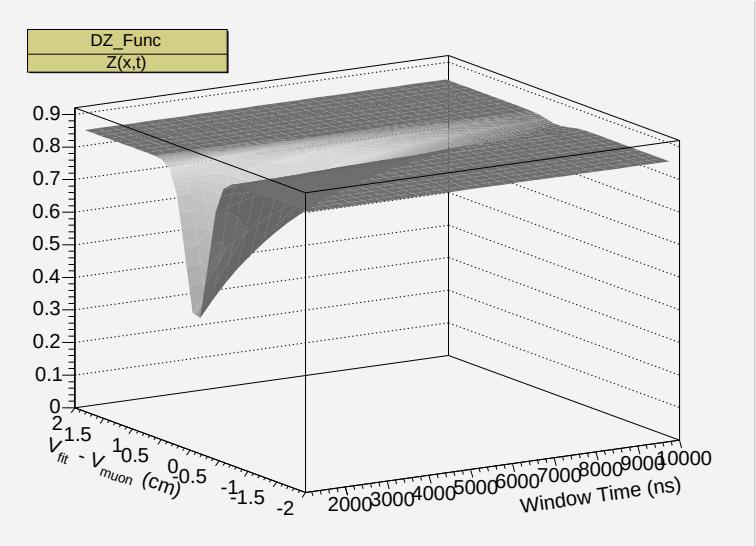

Figure 3.1: Fitting function $Z(x,t)$ for the dead zone parameters found for PC6

The size of the dead zone in PC5, as characterized by the dead length L_{dead}, is smaller than that in PC6 by about 40%. The healing time τ_h is also smaller by approximately 25% in PC5 as compared to PC6. This is expected, because the muon deposits more energy in the wire chamber closer to its decay vertex, thus creating a larger dead zone. Since PC6 is closer to the target, and therefore closer to the muon decay vertex, the dead zone is larger in PC6 than in PC5 (which is adjacent to PC6). Larger dead zones have a larger L_{dead} and a longer τ_h. The results shown here agree with the intuitive understanding of the nature of the dead zone.

3.1 A Study of the Spacial Restriction Tolerance

The tolerance described in the algorithm is needed to restrict the analysis to events in which the effect of the dead zone created in PC5 or PC6 by a muon could possibly have influenced the detection (or non-detection) of a subsequent decay positron. This test was conducted in order to determine whether or not the restrictions made had any effect on the results discussed above. By varying the size of the tolerance and

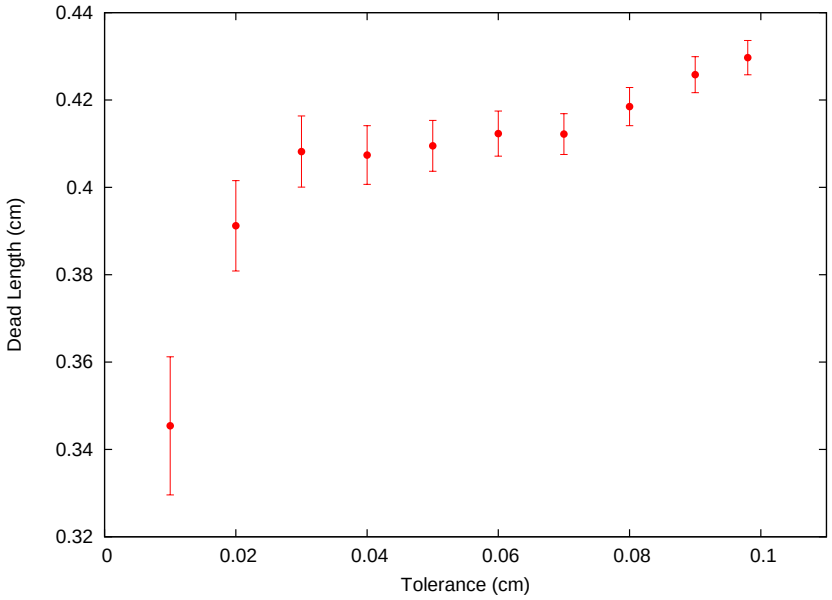

Figure 3.2: L_{dead} dependence on data aquisition tolerance in PC6 for 2×10^7 events

running the analysis program with a total of 2×10^7 events to find the results for L_{dead} and τ_h in PC6, it was possible to plot their dependence on the tolerance size. Ideally, one would hope that L_{dead} and τ_h converge to some constant value within the error of all the calculated values as the tolerance approaches some extremum, making it safe to assume that the extracted results are independent of the tolerance restriction made during data aquisition. The results of this study are plotted in Figures 3.2 and 3.3.

From Figure 3.2, it is clear that L_{dead} varies between 0.34 and 0.43 cm as the tolerance size is increased from 0.01 to 0.10 cm. This is largely due to the small amount of statistics that pass the tolerance criteria at small tolerance sizes. But as the size is of the tolerance is increased, the dead length begins to level off and varies only slightly between $L_{dead} = 0.41$ and 0.43 cm. This is a small enough variation to conclude that L_{dead} is robustly extracted for large tolerance (0.098 cm) and shows no significant dependence on the size of the tolerance (beyond 0.03 cm) implemented in

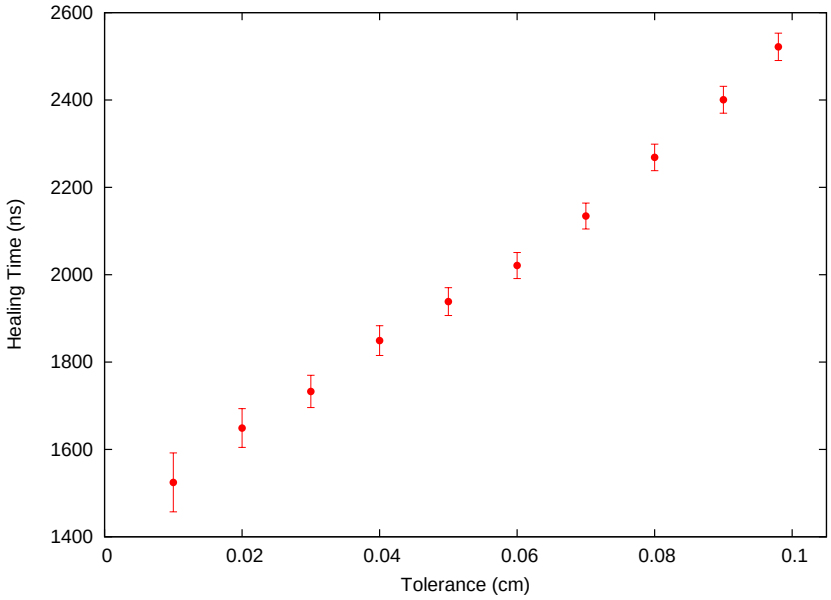

Figure 3.3: τ_h dependence on data aquisition tolerance in PC6 for 2×10^7 events

the analysis. [1]

From Figure 3.3, it is clear that τ_h depends explicitly on the size of the tolerance implemented in the analysis. This is, again, due to the variation in the amount of statistics passing the tolerance criteria, and thus the amount of data being histogrammed. As the window time increases, the probability of recording a decay positron in the desired region decreases exponentially, due to the finite lifetime of the muon. This causes a problem at low statisics because there will not be a well-defined shape of the surface shown in Figure 2.6 at large t-values, it will appear to be flat there. The error assigned to these points (Equation 2.1) is much greater than those at small values of t, so the non-linear least squares fitter (MINUIT) fits a more sharply increasing exponential to the time dependent part of the dead zone function (Equation 2.12). The subsequent effect on the healing time, τ_h, is assigning it a smaller value with a larger error, as shown in Figure 3.3.

[1] One should note that beyond tolerance = 0.10 cm the algorithm described in §2.4 breaks down because it begins to count positron events from adjacent chamber cells. These events are of no interest and only serve to corrupt the events that are of interest.

The error assigned to the extracted fit parameter, τ_h, is also not exactly correct. The fit, as done with MINUIT, did not take into account that the healing time is correlated with the amount of statistics acquired at large t, and thus the size of the tolerance implemented in the analysis. If such a correlated fit was performed the overall effect would be to increase the error on τ_h with an appropriate renormalization factor.

In conclusion, the healing time τ_h cannot be robustly extracted for a single value of the tolerance because the two variables are correlated. A correlated analysis must be done to assign larger errors to τ_h, but an approximation of τ_h can still be made using a large tolerance (0.098 cm) because this guarantees the maximum amount of statistics at large t. Larger statistics implies that the surface at large t will be well-defined, and thus better fit by an uncorrelated analysis.

3.2 The Dead Zone Systematics

The main goal of the analysis outlined in this thesis is to find a systematic uncertainty in the Michel parameters associated with the dead zone in the $\mathcal{TWIST}$ spectrometer. The effect of the dead zone is a loss of positron events during data acquisition. The larger the dead zone and the longer it lasts, and thus the more positron events lost. A characterization of the scale and duration of the dead zone was needed to calculate the associated systematic uncertainty in the Michel parameters.

The results of fits to an MC data set in which the data was correlated (giving a renormalization factor of 0.582) and in which the dead zone effect was exaggerated (giving a scaling factor of 0.1) are as follows: [3]

$$\begin{aligned} \Delta\rho &= 0.0021 \pm 0.0023 \qquad \Delta\eta = 0.1 \pm 0.12 \\ \Delta\delta &= -0.0022 \pm 0.0016 \qquad \Delta\xi = 0.0045 \pm 0.0031 \end{aligned}$$

The calculation of the scaling factor and renormalization factor was done by Dr. Art Olin and other $\mathcal{TWIST}$ collaborators at TRIUMF. The final results of L_{dead} and τ_h, along with their associated uncertainties, were used in this calculation. The renormalization factor—from the correlated analysis—has the effect of reducing the uncertainty in the quantities above, but not on the values themselves. However, the scaling factor—from the exaggeration of the dead zone in the MC data set—reduces both the uncertainty *and* the values. The end result is the systematic uncertainty of the Michel parameters ρ, η, δ and ξ associated with the dead zone effect:

$$\begin{aligned} \Delta\rho &= 0.00021 \pm 0.000134 & \Delta\eta &= 0.01 \pm 0.006984 \\ \Delta\delta &= -0.00022 \pm 0.000093 & \Delta\xi &= 0.00045 \pm 0.000180 \end{aligned}$$

Notice that the systematic error of η is on the order of 10^{-2}. The $\mathcal{TWIST}$ experiment is therefore not as sensitive to η as the other Michel parameters. [2] For more information on the first physical results of $\mathcal{TWIST}$ see the following references: [4], [6].

[2] This is not the only systematic error on η that is above 10^{-4} in the $\mathcal{TWIST}$ experiment.

Chapter 4

Discussion and Conclusion

The questions that were posed as motivation for this study can now be answered:

(1) How large is the dead zone on average?

In PC5: $L_{dead} = 0.2520 \pm 0.0101$ cm.

In PC6: $L_{dead} = 0.4297 \pm 0.0039$ cm.

(2) How long does it take for the dead zone to "heal"?

In PC5: $\tau_h = 1799 \pm 70$ ns.

In PC6: $\tau_h = 2521 \pm 31$ ns.

(3) What is the probability that a positron will go through the dead zone without firing the corresponding wire?

This probability was discovered to be time-dependent, as shown in Figure 2.4. A more appropriate question is: what is the probability that a positron will go through the dead zone without firing its corresponding wire at a time t_o ?

This question can be answered by fitting the histogram shown on the right hand side of Figure 2.4 with a linear function:

$$P(t) = at + b, \tag{4.1}$$

over the range: $1000 \leq t_o \leq 9000$ ns. The fit parameters were found to be:

$a = (5.032 \pm 0.070) \times 10^{-5}$, s^{-1}

$b = (-0.01645 \pm 0.00195)$.

So, for example, at a time half way through the event window: $P(4000\text{ ns}) = 0.185 \pm 0.003$ where the uncertainty in the probability is given by:

$$\delta P(t) = \sqrt{(\delta a)^2 t^2 + (\delta b)^2} \tag{4.2}$$

But this is a measure of the probability that a positron *will* fire a wire in the dead zone, so the probability that the positron *will not* fire a wire in the dead zone is: $1 - P(t) = 0.815 \pm 0.003$.

(4) What effect does this dead zone have on the analysis of the Michel parameters? i.e. what is the systematic uncertainty of the Michel parameters associated with the dead zone?

As stated in §3.2, the associated systematic uncertainties on the Michel parameters are:

$$\begin{array}{llll} \Delta\rho = 0.00021 \pm 0.000134 & \Delta\eta = 0.01 \pm 0.006984 \\ \Delta\delta = -0.00022 \pm 0.000093 & \Delta\xi = 0.00045 \pm 0.000180 \end{array}$$

At present, the $\mathcal{TWIST}$ group has published their first results of the Michel parameters at the 10^{-3} level. [6], [4]. In order to ensure that this experiment can continue on to the 10^{-4} level they must be sure that their systematics are lower than a few parts in 10^5, otherwise the Michel parameters will be limited by the systematics of the experiment. This can be accomplished by going to higher statistics, which requires more data.

This study has shown evidence of a time-dependence on the efficiency of proportional counters when dealing with large energy loss. Using a muon beam where the muons are incident on the spectrometer at some rate, r, the creation and destruction of a dead zone near the end of the muon lifetime will be periodic *only if* the healing time of the dead zone is less than the period of incident muons $(1/r)$. If τ_h is larger

than the period of incident muons, the dead zone will not have sufficient time to completely heal and it will continually grow in size until some upper limit is reached. At this point, the dead zone will essentially exist in the proportional counter until a sufficient change in the muon beam rate allows it to heal. This is not good for the efficiency of the proportional chambers, because they become insensitive to charged particle traversal in the "dead" region for as long as the dead zone exists.

This study has also shown that the dead zone can be characterized by two main parameters: L_{dead} and τ_h. Approximations of these two parameters can be made by using a simple selection algorithm, such as that described in §2.4, and performing an uncorrelated fit to the data using an empirically derived function (Equation 2.12). However, more accurate results can be obtained using a correlated fitting algorithm since the healing time parameter τ_h is correlated to the total number of data points used in the fit.

Acknowledgements

I would like to acknowledge and thank the following people for their help in the development of this thesis:

- Dr. Adam Sarty for his supervision at Saint Mary's and the many hours he put in to revising and editing the first drafts of this thesis.
- Dr. Art Olin for his supervision at TRIUMF and his unique teaching method of "throwing me in with the wolves"!
- Dr. Glen Marshall and Dr. David Gill for their support and guidence at TRIUMF and introducing me to the $\mathcal{TWIST}$ experiment.
- The following people deserve special mention, as they all provided me with professional and courteous help on countless occasions concerning the nitty-gritty details of $\mathcal{TWIST}$s data analysis framework.
  - Andrei Gaponenko
  - Dr. Jingliang Hu
  - Blair Jamieson
  - Robert MacDonald
  - Dr. Dick Mischke
  - Jim Musser
  - Dr. Konstantin Olchanski
  - Dr. Maher Quraan

Bibliography

[1] R. Brun and F. Rademakers. Root: An object oriented data analysis framework. Website: http://root.cern.ch/, 2004. Retrieved July, 2004.

[2] TWIST Collaboration. Information for the general public. Website: http://twist.triumf.ca/, 2004. Retrieved May, 2004.

[3] TWIST Collaborators. Twist 2002/2003 data analysis—systematics review. Private communication, March, 2005.

[4] A. Gaponenko et al. Measurement of muon decay parameter δ. Website: http://www.triumf.info/, 2005. Accepted to Physical Review D, March 2005.

[5] D.E. Groom et al. Review of particle physics. *The European Physical Journal*, C1, 2000.

[6] J.R. Musser et al. Measurement of the michel parameter ρ in muon decay. *Physical Review Letters*, 94, 2005.

[7] R. Brun et al. Root users guide 3.10. Website: http://root.cern.ch/root/doc/RootDoc.html, January 2004. Retrieved July, 2004.

[8] W. H. Press et al. *Numerical Recipes in Fortran 77: The Art of Scientific Computing*, volume 1. Cambridge University Press, Cambridge, 2nd edition, 2003.

[9] W. R. Leo. *Techniques for Nuclear and Particle Physics Experiments: A How-To Approach.* Springer-Verlag Berlin Heidelberg, 2nd edition, 1994.

[10] TRIUMF. Triumf backgrounder. Website: http://www.triumf.info/public/about/background.html, 2004. Retrieved October, 2004.

[11] TRIUMF. Triumfs public website. Website: http://www.triumf.info/, 2004. Retrieved January, 2005.

[12] D. G. Zills and M. R. Cullen. *Differential Equations with Boundary-Value Problems.* Brooks/Cole, Pacific Grove, CA, USA, 5th edition, 2001.